Liu rong[1,2] , Li ji-sheng[2] , Fan yang-yu[1],Tian wei-jian[1]
1.School of Electronics and Information, North western Poly technical University
2.College of Physics and Information Technology ,Shaanxi Normal University

Detection of PD under Oscillatory Impulse Voltage

Abstract. *In order to study the partial discharge (PD) pulses under oscillatory impulse voltage (OIV), an oscillation waveform generator is designed and the waveform parameters expressions are presented based on the equivalent circuit model. A high-frequency current transducer is developed for measurement of PD. Then the effects of coil turns and integral resistance on frequency properties are studied. Moreover, calibration and analysis of the actual dynamic response are performed by adopting function generator and square-wave source. The PD measurement system to detect the PD signals of needle-plate model under OIV is provided finally. Experiment shows that by adapting this PD measurement system, the source interferences are restrained and PD signals are effectively extracted, therefore it could be a worthy approach not only for further study on PD character under OIV, but also to explore the mechanism behind it.*

Streszczenie. *Zaprojektowano generator napięć impulsowych przeznaczony do badań wyładowań niezupełnych pod wpływem napięć impulsowych. Zaprojektowano też wysokoczęstotliwościowy czujnik prądu. Wyładowania niezupełne badano w układzie miedzy ostrzem a płaszczyzną. Uzyskano eliminację sygnału interferencji i dobrą ekstrakcję sygnału wyładowania. (**Detekcja wyładowań niezupełnych powstających pod wpływem napięcia impulsowego**)*

Keywords: partial discharge; oscillatory impulse voltage; high-frequency current transducer; mechanism.
Słowa kluczowe: wyładowania niezupełne, napięcie impulsowe, czujnik prądu.

Introduction

In recent years, partial discharge (PD) measurement has become an important means of electrical equipment insulation monitoring [1]. PD detection can be carried out during the process of the withstand voltage test on power equipment, and this technique has reached a comparatively mature stage. However, with the constant improvement of the voltage grade, the oscillatory impulse withstand voltage test becomes necessary to inspect the insulation strength of the power equipment on site. Moreover, it is especially effective to diagnose the existence of pollution and abnormal electric field under oscillatory impulse voltage (OIV). According to the IEC60060-3 standard [2], PD diagnosis under OIV has important practical significance to detect hidden trouble and ensure the safe operation of the equipment. Therefore, studying PD measurement technique under those impulse voltages has an important engineering application value.

According to IEC 60270 [3], the conventional method for PD detection is based on the precondition that the frequency contents between the PD and the applied voltage are totally different, which can be used for separation between the PD and applied voltage. However, detection of PD signals under impulse voltage becomes more difficult due to the high frequency interferences produced by the applied voltage. In such cases the conventional PD measuring method cannot meet measurement requirements. This situation calls for a new detection technique for the measuring systems used. Up to present, researches on PD under impulse voltage have been focused on the following aspects. One is the optical measurement method [4-7], which is unsuitable for on site detection due to its own defects. Another approach is to use filtering technique that effectively suppresses the contribution from the applied voltage [8].

The aim of this paper is to design an OIV generator which can produce waveform that is coincident with the IEC60060-3 standard firstly. Then a new high frequency Micro-current transducer is set up, and based on which a PD measuring system is developed. Experiment results from measurements on corona discharge of needle-plate electrode under OIV show that this system is efficient in PD detecting and weakening interferences.

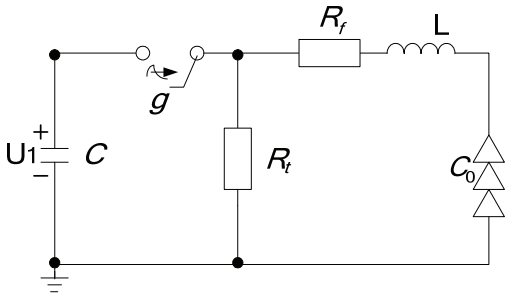

Fig.1. The schematic OIV generator (C, generator capacitor; R_f and R_t, shaping resistors; C_o, load capacitance ;g, spark gap; U_1, the initial voltage)

Experiment setup

Designing of the OIV generator

A schematic diagram of the generator is shown in Fig. 1.The generator capacitor C was pre-charged and then isolated from the DC source. The oscillatory impulse was generated by the gap g breakdown. On the assumption that the system was in underdamping state, the voltage of the load capacitor C_0 (consists of sample and voltage divider capacitor) corresponding to the front-time of the waveform could be calculated as equation (1).

(1) $$u_2(t) = U[1-(\omega_0/\omega)\exp(-\alpha t)\sin(\omega t+\varphi)]$$

Where $U = CU_1/(C+C_0)$, $\alpha = R_f/(2L)$, $\omega_0 = 1/(LC_1)^{1/2}$, $\omega = (\omega_0^2-\alpha^2)^{1/2}$, $\varphi = \arctan(\omega/\alpha)$, $C_1 = CC_0/(C+C_0)$.

Deriving of the equation (1), we could obtain the front time T_f corresponding to $u_{2\max}(t)$ as follows.

(2) $$T_f = \pi/\omega = \pi/(\omega_0^2-\alpha^2)^{1/2} \approx \pi\sqrt{LC_1}$$

The oscillation frequency of the waveform f is

(3) $$f = (\omega_0^2-\alpha^2)^{1/2}/(2\pi) \approx 1/2\pi\sqrt{LC_1}$$

Also, from Fig.1, we could deduce the envelope equation of the waveform as follows.

(4) $$u(t) = 2C_1U_1(1+\exp(-R^{'}/2L)T_f)*\exp(-t/R^{'}(C_0+C)$$

Where $R^{'} = R_t + R_f$.

From formula (4), the time to half-value T_t in $u(T_t) = \frac{1}{2}u_{\max}$ is given by

(5) $$T_t \approx 0.25 * R^{'} C_1$$

In the experiment, one of the defined waveforms by IEC60060-3 standard was chose as the objective. The parameters of the waveform are as follows: $T_f = 1\mu s$, $T_t = 50\mu s$, $f = 370KH_z$. C=0.033 μF and C_0 =500 pF were selected. Based on the equations (2), (3) and (5), the value of residual components of the generator could be calculated as $L = 2mH$, $R_f = 0.5K\Omega$, and $R_t = 3.2K\Omega$ respectively. Fig.2 describes the output waveform of the generator, which was measured by a 500MHz digital storage oscilloscope of DPO4054 with a sampling frequency of 2.5GS/s. From Fig.2, the following parameters could be measured: $T_f = 1.2\mu s$, $T_t = 48\mu s$ and $f = 368KH_z$. All of the results are within the accepted error range and meet test requirement.

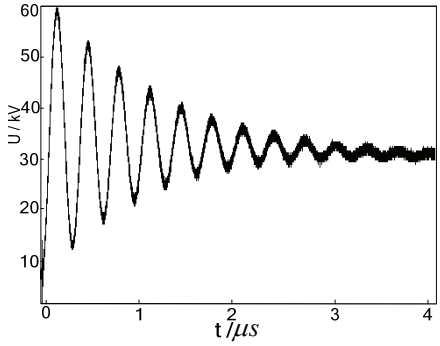

Fig.2. The OIV waveform

A. Designing of the high frequency current transducer

The designed current transducer works on the principle of electromagnetic coupling. A schematic diagram of the transducer is shown in Fig. 3[9]. It was placed around the conductor to couple the pulse signals.

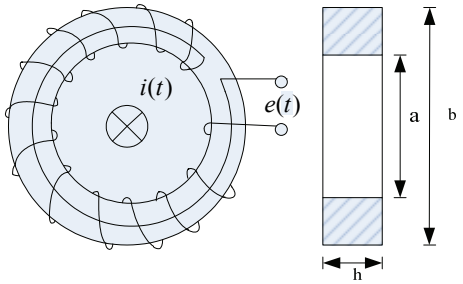

Fig.3. The schematic diagram of the transducer (a, inner diameter of coil; b, the outer diameter of coil; h, the thickness of coil; $i(t)$, the original current; $e(t)$,output voltage of the transducer)

The following equation could be deduced from Fig.3:

(6) $$e(t) = -M \frac{di(t)}{dt}$$

Where M is the mutual self-inductance of the coil.

B. Selection of the magnetic core

The frequency range and configuration parameters of the magnetic core play an important role in determining bandwidth (BW) of the current transducer. The studies of frequency response characteristics of different magnetic cores have been presented in literature [10], experiment results showed that a type of ferrite of nickel-zinc material with high resistivity and low coercive force can be used to obtain the performance of broadband and lower loss. Therefore, nickel-zinc core was selected in the design of transducer, and the parameters of core are: $a = 26mm$, $b = 45mm$, $h = 15mm$, μ (magnetic permeability)=10. There was no need to consider the saturation problem of the magnetic core owing to the measured PD current at the level of milliampere.

C. Selection of R and N

R and N are the main parameters that have a great effect on BW besides of magnetic core. The instrument for experiments is an arbitrary waveform generator AWG2021, which can generate a sine wave from 10Hz to 125MHz with amplitude of 0 to 5V and a calibrating square wave with amplitude of 0 to 5V. The measuring circuit is shown in Fig. 4. All the data were measured with a 200MHz digital storage oscilloscope of DPO2022B. Fig.5 shows the frequency response of the transducer when changing the value of the R and N respectively.

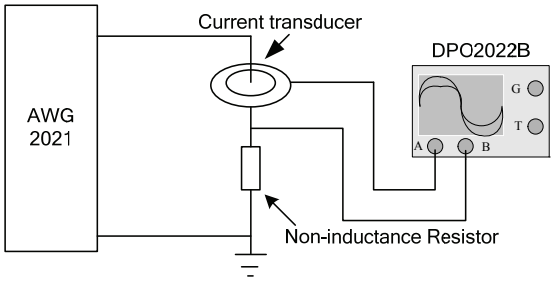

Fig. 4. The measuring circuit for response characteristics of the current transducer

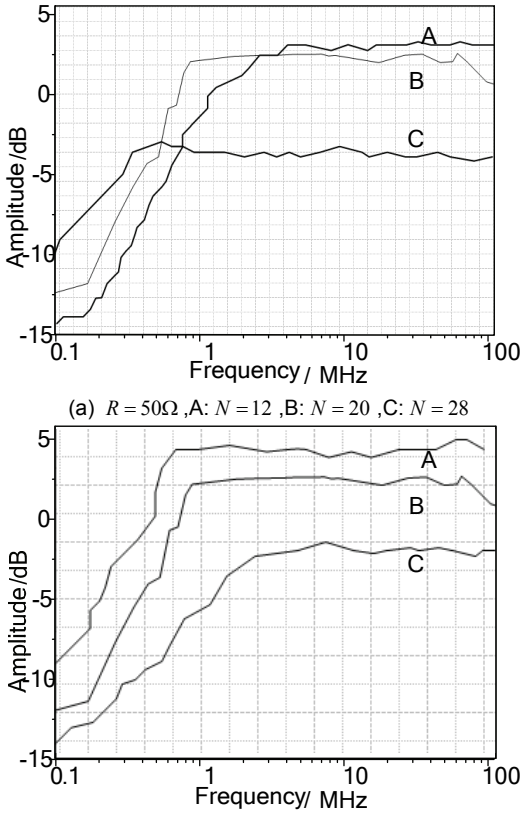

(a) $R = 50\Omega$,A: $N = 12$,B: $N = 20$,C: $N = 28$

(b) $N = 20$,A: $R = 100\Omega$,B: $R = 50\Omega$,C: $R = 10\Omega$

Fig. 5. The amplitude-frequency response characteristics of the current transducer

From the Fig.5, it can be found that the sensitivity is enhancing by increasing R . However, the low limiting frequency increases while the upper limiting frequency decreases. Thus, BW can be diminished with a high value of R . It can also be found that the BW becomes larger with the increase of N , but the sensitivity becomes lower. Therefore, it is necessary to optimize the values of R and N to meet the requirements of appropriate sensitivity and BW.

Based on the experimental results, the best parameters are as follows: $N = 20$, $R = 50\Omega$ for the wide bandwidth of 800 KHz~105MHz and high sensitivity of 2.4VA^{-1}.

D. Tests of the designed high frequency current transducer

The amplitude-frequency response and the step wave response are two important items of the dynamic characteristics. Fig. 6(a) shows the square wave response of the transducer. The fall time of calibrating square wave (CH1) and the high frequency current transducer are about 2.13ns and 3.43ns respectively. So the upper frequency calculated by equation (7) of the transducer is about 92.8MHz, which matches well the amplitude-frequency response. The current transducer adopted to measure the calibrating pulse is shown in Fig. 6(b). CH1 and CH2 are the calibrating waveform and the response waveform respectively. It can be seen that the waveforms are almost the same in their rise time, which indicates that the current transducer can be used to measure nanosecond pulse signals effectively.

(7) $$f_H = \frac{1}{\pi t_{rise}}$$

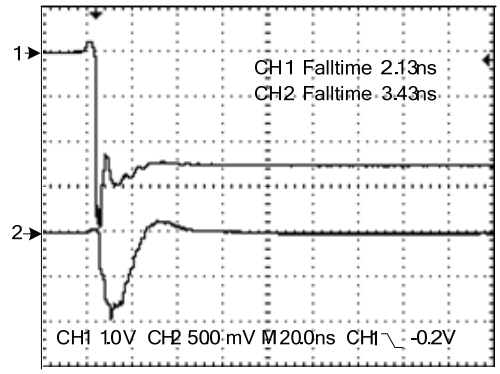

(a) The square response of the transducer

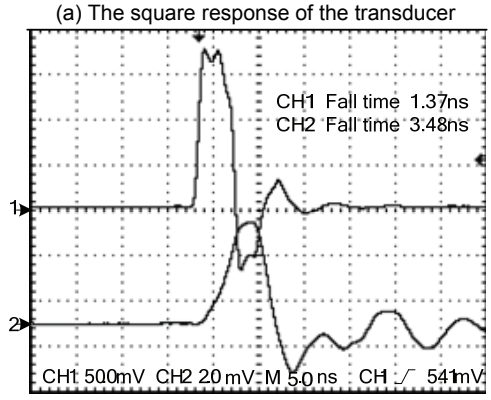

(b) The measurement of the high frequency pulse

Fig. 6. The actual dynamic responses of the transducer

Measurement of PD signals under OIV

Fig. 7 shows the experimental system for PD measurements under OIV. A needle electrode with a tip radius of 1mm and a length of 20 mm was connected to the generator. The diameter of the ground electrode is 80 mm and the gap length of the needle-plate electrode is 50 mm. The experiment tank was filled with SF6 gas and the pressure reached $P = 0.2$ MPa. The 50% probability PD inception voltage was determined by the up-and-down method. A time interval of 3 min was allowed between the adjacent impulse voltage applications to reduce the influence of the residual space charges. PD current pulse waveforms were measured by DPO4054 through the designed high-frequency current transducer. A high pass filter was adopted to eliminate the impulse noise and displacement current caused by the impulse voltage. The sensitivity of this PD current detection system was dozens of pC. In addition, the PD light intensity was measured using a photomultiplier tube (PMT). All the above experiments were carried out at room temperature.

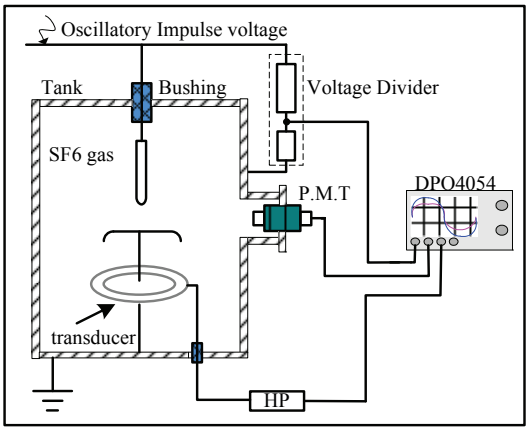

Fig. 7. Experimental setup.

Fig. 8 shows the PD current and light intensity waveforms in SF6 gas under oscillatory impulse waveform at $P = 0.2$ MPa. The multi-peak pulses of the PD current and light intensity were observed indicating the occurrence of the impulse PD under the impulse voltage.

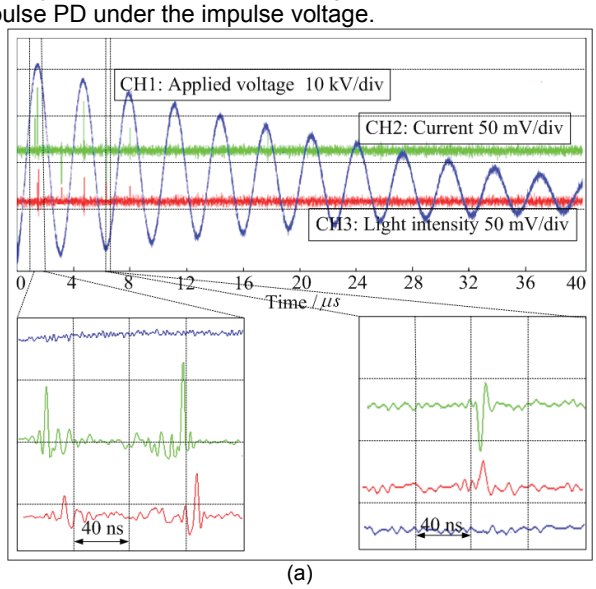

(a)

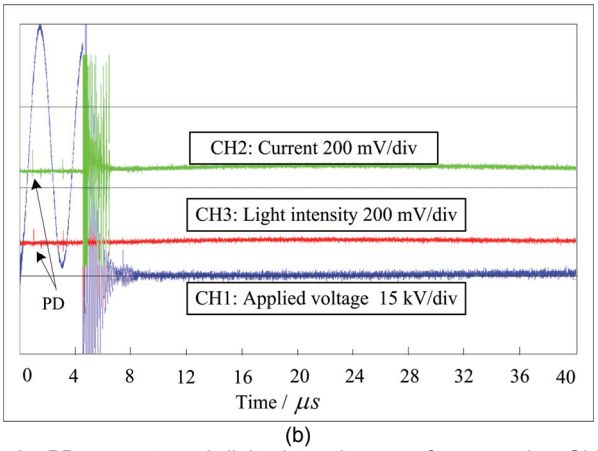

(b)

Fig. 8. PD current and light intensity waveforms under OLI application at $P = 0.2$ MPa: (a) Breakdown did not happen ($V_{CH1} = 39$ kV); (b) Breakdown happened ($V_{CH1} = 46$ kV).

Considering the stochastic nature of the PD, the data of the PD characteristics were obtained by performing large numbers of PD measurements. Based on the PD characteristics data, we drew the following conclusions:

(1) Most of the PD signals appeared in the first few cycles of the OIV waveform. In addition, the PD signal with the maximum amplitude occurred at the peak or trough of the OIV waveform. The occurrence of the PD signal at the trough can be explained by the following mechanism: the space charges from the streamer corona discharge are accumulated around the needle tip at each peak of the oscillating impulse waveform, and then a reverse electrical field is formed by the space charges as the applied voltage decreases rapidly. Thus, the back discharge occurs when the strength of the reverse electrical field reaches a critical one.

(2) High amplitude PD signals appeared during the pre-breakdown under OIV. The breakdown frequently occurred at the peak of the first few cycles of the OIV waveform.

Discussion

Based on the above experimental results, the characteristics and mechanisms of PD and breakdown under the four impulse voltages were discussed as follows:

(1) Various mechanisms are possibly involved in the breakdown of the non-uniform field gap of SF6 gas, such as the stem mechanism, precursor mechanism and high frequency mechanism. The precursor mechanism plays a dominant role in the breakdown propagation under the aperiodic impulse voltage [11-13]. A brief description of the precursor process is given as follows: The positive and negative ions released by the plasma layer of the corona streamer are subjected to an external electrical field and start to drift in the opposite directions, respectively. This drift results in the charge separation and the formation of space charge polarization, which is accompanied by a local electric field enhancement. As a result, ionization re-occurs in the plasma zones of the enhanced electric field, which results in a current through the space charge filament. After that, the discharge propagation stops due to the space charge shielding. However, the space charge shielding decreases with the thermal expansion of the streamer plasma channel and the diffusion and drift of the space charge, which leads to further ionization at the end of the channel and a stepwise elongation of the filament. Eventually, the filament reaches the electrode, indicating the breakdown of the gap.

(2) The discharge behavior under OIV is not subjected to the above analysis of the precursor mechanism due to the influence of oscillation. When the oscillation frequency is high, the discharge in SF6 gas is affected by a combination of the high frequency and precursor mechanisms[14]. Therefore, the energy for the streamer-to-leader transition is provided by the corona streamer current and the displacement current generated as a result of high frequency oscillation. Fig. 9 shows the model for high frequency mechanism.

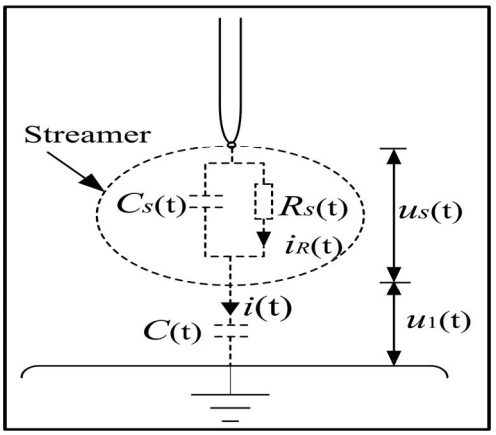

Fig. 9. High frequency mechanism.

The displacement current $i(t)$ in the high frequency mechanism can be expressed as:

$$i(t) = c(t) \cdot \frac{du_1(t)}{dt} + u_1(t)\frac{dc(t)}{dt} = i_R(t) + \varepsilon \frac{du_s(t)}{dt} \tag{8}$$

where ε is the permittivity.

The energy to maintain the ionization can be calculated as:

$$W = \int u_s(t) i_R(t) dt \tag{9}$$

The equivalent capacitance C between the discharge channel and plate electrode increases with the development of the discharge channel in the model for the high frequenc y mechanism (Fig. 9), which leads to the increase in the dis placement current i and the current i_R flowing through the equivalent resistance of discharge channel. Accordingly, the temperature within the discharge channel and the energy u sed to maintain the channel are both enhanced, which ultim ately promotes the ionization.

Conclusion

Based on the analysis of the equivalent circuit of OIV generator, the relationship between waveform parameters and circuit elements were deduced. It was beneficial to produce the needed waveform through choosing appropriate parameters of the elements. A high frequency current transducer was designed to have both BW and high sensitivity by proper selection of the three main parameters through analysis of the magnetic core effect on the bandwidth of the current transducer as well as the effect of R and N. Moreover, the PD experimental system was developed based on the current transducer. The experiment results show that the current transducer can correctly reproduce the waveforms of PD pulses with nanosecond rise time and lower amplitude, and suppress the interference produced by applied voltage effectively. They

are useful for further study of PD and breakdown characteristics under OIV.

The PD measurement techniques used in this study under impulse voltages, together with the discussion of the PD inception voltage and the breakdown characteristics, are expected to contribute to defect diagnosis of GIS during the on- site withstand voltage test.

Financial support from the Natural Science Foundation of China (No 50977075*) is gratefully acknowledged.*

REFERENCES

[1] Hitoshi Okubo．Recent Progress and Future Perspective on Condition Monitoring and Diagnostic Techniques for Power Equipment in Japan[C] ． Proceeding of International Conference on Condition Monitoring and Diagnosis，Beijing，China，2008．

[2] IEC 60060-3 High voltage test techniques part 3：definitions and requirements for on-site tests[S]，2005．

[3] IEC Standard Publication 270 ． Partial Discharge Measurements[S]．Second Edition，1981．

[4] K Yamazawa，M Uemura，H Yamashita，E O Forster．Pulse Measurements Using LED in Dielectric Liquids under Impulse Voltages[J]．IEEE Transaction on Dielectrics and Electrical Insulation，1994，1(3)：391-396．

[5] M．Kaufhold，S．S．Bamji，A．T．Bulinski．Optical Detection of Partial Discharges in Gas-Insulated Systems[C]．Conference on Electrical Insulation and Dielectric Phenomena，San Francisco，1996．

[6] Naoki Hayakawa，Yuichiro Yoshitake，Naoto Koshino，et al．Impulse Partial Discharge Characteristics and Their Mechanisms under Non-uniform Electric Field in N2/SF6 Gas Mixtures[J]．IEEE Transactions on Dielectrics and Electrical Insulation，2005，12(5)：1035-1041．

[7] B.H. Tan, N.L. Allen, H.Rodrigo. Progression of Positive Corona on Cylindrical Insulating Surfaces Part I: Influence of Dielectric Materical[J]. IEEE Transactions on Dielectrics and Electrical Insulation，2007, 14(1)：111-118．

[8] Elisabeth Lindell，Tord Bengtsson，Jorgen Blennow，Stanislaw M Gubanski．Measurement of Partial Discharges at Rapidly Changing Voltages[J]．IEEE Transactions on Dielectrics and Electrical Insulation，2008，15(3)：823-830．

[9] WANG Changchang, LI Fuqi, GAO Shengyou, etal. On-line Monitoring and Diagnosis for Power Equipment [M]. University of Tsinghua Press, Beijing, 2006.

[10] Q Zhang，J Zhu，J Jia，et al．Design of a current transducer with a magnetic core for use in measurements of nanosecond current pulses[J]．Meas. Sci. Technol．2006，17：895-900．

[11] I. Gallimberti and N. Wiegart, " Streamer and leader formation in SF6 and SF6 mixtures under positive impulse condition", Pts I and II,J.Phys.D: Appl.Phys. Vol.12.pp.2351-2379,1986.

[12] L. Niemeyer, L. Ullrich, and N. Wiegart, " The mechanism of leader breakdown in electronegative gases" , IEEE Trans. Electr. Insul., Vol.24, pp. 309-324, 1989.

[13] Wiegart, N., L. Niemeyer, F. Pinnekamp, W. Boeck, J. Kindersberger, R. Morrow, W. Zaengl, M. Zwicky, I. Gallimberti, and S.A. Boggs. "Inhomogeneous Field Breakdown in GIS - The Prediction of Breakdown Probabilities and Voltages. Part I, II, and III, IEEE Trans. Power Delivery, Vol. 3, pp. 923-946,July.1988.

[14] D. Buchner, " Breakdown of SF6 insulation in case of inhomogeneous fields under different transient voltage stress", 9th ISH, 1995.

Corresponding author*: Lecturer Li Jisheng, College of Physics and Information Technology ,Shaanxi Normal University, Xi'an, Shaanxi, China,710062, E-mail: jishengli2011@163.com;*